

# Filter comparison for estimation on discretized PDEs modeling traffic: Ensemble Kalman filter and Minimax filter

Toru Seo, Tigran T. Tchraikian, Sergiy Zhuk, and Alexandre M. Bayen

**Abstract**—*Traffic State Estimation (TSE) refers to the estimation of the state (i.e., density, speed, or other parameters) of vehicular traffic on roads based on partial observation data (e.g., road-side detectors and on-vehicle GPS devices). It can be used as a component in applications such as traffic control systems as a means to identify and alleviate congestion. In existing studies, the Kalman Filter and its extensions, notably the Ensemble Kalman Filter (EnKF), are commonly employed for TSE. Recently, the MF has been newly adapted to this domain as a filtering algorithm for TSE. In this article, we compare the performance of the EnKF and the MF on discretized PDE models of traffic flow traffic. Specifically, for the EnKF study, the estimation is performed using stationary and mobile sensor information based on actual traffic data, by employing EnKF in conjunction with a Godunov discretization of the Lighthill–Whitham–Richards (LWR) model. For the minimax study, the discontinuous Galerkin formulation of the LWR model is used in conjunction with the implicitly-linearized MF to obtain state estimates using the same data. The advantages and disadvantages of each of the filters are empirically quantified. Insights for practical application and future research directions are presented.*

## I. INTRODUCTION

Traffic State Estimation (TSE) refers to the estimation of density, speed, or other parameters of vehicular traffic on roads based on partial observation data (e.g., road-side detectors and on-vehicle GPS devices). It can be used as a component in applications such as traffic control systems as a means to identify and alleviate congestion [1]. Since observing the state everywhere is not practically feasible, TSE is usually performed based on partial observation data, such as measurements of road-side detectors, i.e., stationary data, and using in-vehicle Global Positioning System (GPS) devices, i.e., mobile data.

Vehicular traffic dynamics can be modeled macroscopically using Partial Differential Equations (PDEs). The most basic macroscopic model is the *Lighthill–Whitham–Richards* (LWR) model [2], [3], which consists of a scalar conservation law. Although the LWR model is relatively simple, it can reproduce some of essential phenomena in traffic, such as congestion. In addition, its compactness leads to efficient and accurate numerical schemes to approximate its solution, such as the Godunov scheme [4], [5].

T. Seo is with Transport Studies Unit, Tokyo Institute of Technology, 2-12-1-M1-20, O-okayama, Meguro, Tokyo 152-8552, Japan [t.seo@plan.cv.titech.ac.jp](mailto:t.seo@plan.cv.titech.ac.jp)

T. T. Tchraikian and S. Zhuk are with IBM Research – Ireland, IBM Technology Campus, Damastown, Mulhuddart, Dublin 15, Ireland. [{tigran, sergiy.zhuk}@ie.ibm.com](mailto:{tigran, sergiy.zhuk}@ie.ibm.com)

A. M. Bayen is with Electrical Engineering and Computer Sciences, Institute of Transportation Studies, University of California, Berkeley, 109 McLaughlin Hall, Berkeley CA 94720-1720 [bayen@berkeley.edu](mailto:bayen@berkeley.edu)

In existing TSE studies, the Kalman filter and its extensions are commonly employed, for example, [1], [5]. In these works, the system model consists of discretized PDEs describing the traffic flow. In particular, Ensemble Kalman Filter (EnKF) [6] combined with the LWR model discretized by the Godunov scheme has received attention due to its ability to handle nonlinearity in traffic [5].

Recently, the use of a Minimax Filter (MF) was proposed for the TSE problem [7]. For this, the traffic flow model was solved using the Fourier–Galerkin spectral method. While the numerical convergence results based on the experiments looked promising, the Fourier–Galerkin method required the use of periodic boundary conditions, restricting its applicability in practice. In a subsequent work [8], this issue was addressed by developing a macroscopic traffic data-assimilation algorithm which employed a different Galerkin method in place of Fourier–Galerkin, namely, the discontinuous Galerkin method; and this allowed the incorporation of more general boundary conditions. The convergence of this filter has been studied in [9] and in [10] assuming that the model is bilinear as it is the case for LWR model subject to periodic boundary conditions.

The aim of the present article is to compare performance of the MF and the EnKF for TSE on experimental data, and to obtain insights on practical application and future theoretical research from it. To do so, we compare the performance of EnKF and the MF on discretized PDEs modeling traffic. In order to compare them in a context relevant for practical applications, stationary and mobile sensor information based on actual traffic data are employed. We note that so far, the MF has not been applied to actual traffic data in any existing studies.

The rest of the article is organized as follows. Sections II and III describe the TSE methods using the implicitly-linearized MF [8] and EnKF [5], respectively, based on the LWR model. Section IV describes specification of the data employed for our verification. Section V describes empirical comparison results. Section VI concludes this article.

## II. MINIMAX FILTER FOR LWR MODEL

In this section, we describe the TSE approach based on the *Discontinuous Galerkin* (DG) weak formulation of the LWR model and MF.

### A. Traffic flow model

The LWR model is given by the PDE,

$$\partial_t \rho(x, t) + \partial_x f(\rho(x, t)) = 0, \quad (1)$$

with initial data

$$\rho_0(x) = \rho(x, 0), \quad (2)$$

and boundary conditions,

$$\rho(0_-, t) = g(t), \quad \rho(L_+, t) = h(t). \quad (3)$$

The scalar valued function,  $\rho : \mathbb{R} \times \mathbb{R}_+ \rightarrow \mathbb{R}$  is the traffic density. The flux function is given by  $f : \mathbb{R} \rightarrow \mathbb{R}$ , and the independent variables,  $x \in \mathbb{R}$  and  $t \in \mathbb{R}_+$  denote space (along roadway) and time respectively. We use the quadratic flux function

$$f(\rho) = \rho v_{\max Q} (1 - \rho/\rho_{\max Q}), \quad (4)$$

where  $\rho_{\max Q}$  and  $v_{\max Q}$  are the maximum density and maximum attainable speed respectively, and,  $\rho \in [0, \rho_{\max Q}]$ .

### B. Discretized computational scheme for the model

The formulation described in this section follows [7] except for the numerical flux, which we will address later. For the sake of brevity, we will present only the key details. For a more detailed description of the formulation, see [7].

Before writing the weak DG formulation for the LWR model, we must first present a few definitions. We wish to solve the LWR model, (1), for  $t > 0$  on the space interval  $x \in [0, L] = \Omega$ . In the DG method,  $\Omega$  is first divided into  $K$  non-overlapping elements,  $x \in [x_l^k, x_r^k] = D^k, k = 1, \dots, K$ , i.e.,  $x_l^k$  and  $x_r^k$  are the left and right boundaries of element  $D^k$  respectively. The density,  $\rho$ , and flux,  $f$  are expanded in a basis of Lagrange interpolating polynomials,  $\ell_i(\cdot)$ . The projection coefficients in this basis are simply values of the function being expanded at a specified set of points. The actual values of the functions  $\rho$  and  $f$  on element  $k$  are denoted by  $\rho^k(x, t)$  and  $f^k(x, t)$ , and the projection coefficients of these in the Lagrange basis are denoted by  $\rho^k(x_i, t)$  and  $f^k(x_i, t)$ , where  $x_i$  are a set of integration points on the element with  $i = 1 \dots N + 1$ .

The weak DG formulation of LWR is given by

$$M^k \frac{d}{dt} \rho_h^k - S^T \mathbf{f}_h^k = - [\ell^k(x) f^*]_{x_l^k}^{x_r^k}, \quad (5)$$

where  $\rho_h^k = (\rho^k(x_1, t), \dots, \rho^k(x_{N+1}, t))^T$ ,  $\mathbf{f}_h^k = (f^k(x_1, t), \dots, f^k(x_{N+1}, t))^T$ ,  $\ell^k(x) = (\ell_1^k(x), \dots, \ell_{N+1}^k(x))^T$ , and

$$M_{ij}^k = \frac{h^k}{2} \int_I \ell_i(\xi) \ell_j(\xi) d\xi, \quad S_{ij} = \int_I \ell_i(\xi) \frac{d\ell_j(\xi)}{d\xi} d\xi,$$

are known as the mass and stiffness matrices respectively. The variable,  $\xi$  is a local variable on the ‘‘standard’’ elemental interval. The change of variable from standard to physical intervals using the associated mapping gives rise to the metric constant,  $\frac{h^k}{2}$  which appears in the expression for the mass matrix, where  $h^k$  is the physical length of the  $k$ -th element. The term on the right hand side of (5) is responsible for inter-element fluxes, where  $f^*$  is the numerical flux function. See [7] for full details on this formulation and for more details regarding the DG method in general, see [11].

For the purpose of data assimilation, we express the weak DG formulation of the LWR model in the following form:

$$\frac{d\omega}{dt} = A(\omega)\omega + B(t) + e^m(t), \omega(0) = \omega_0 + e^b \quad (6)$$

This is the global system obtained by assembling the  $K$  elemental systems given by (5). The state vector,  $\omega$ , is thus composed of the elemental state vectors,  $\rho_h^k$ . The matrix,  $A(\omega)$  in this work differs from that in [7] due to the choice of numerical flux function. Specifically, we now employ the local Lax–Friedrichs flux instead of the Godunov flux. As a result,  $A(\omega)$  absorbs all of the inter-element flux terms. The fluxes at the boundaries, however, appear in  $B(t)$  and are state-independent.  $e^m$  represents model error which absorbs both numerical and physical model errors and  $e^b$  describes the error in the initial condition.

The observation equation for the system is given by,

$$Y(t) = H\omega(t) + \eta(t), \quad (7)$$

where  $H$  is an observation operator and  $Y : \mathbb{R} \rightarrow \mathbb{R}^M$  is an  $M$ -element vector containing observations at time,  $t$ . The vector,  $\eta$ , is a noise term which accounts for the error in measurements. As the state vector,  $\omega$ , is composed of grid functions,  $\rho_h^k$  over integration points on elements, the operator,  $H$ , attains a simple form: if measurements are available at all grid-points, then  $H$  is the identity matrix. If the number of available observations,  $M$ , is less than the total number of grid-points, the matrix  $H$  comprises only the corresponding  $M$  rows of the full  $H$  (identity matrix).

### C. Minimax filter

In the minimax framework, the initial state-, model- and measurement-error terms,  $e^m$ ,  $e^b$  and  $\eta$  can be used to define the model and error covariance matrices,  $t \mapsto Q(t)$  and  $t \mapsto R(t)$ . For details on this, see [7]. We further assume that the initial state-, model- and measurement-error terms,  $e^m$ ,  $e^b$  and  $\eta$  verify the following inequality:

$$(e^b)^T S e^b + \int_0^T (e^m)^T Q e^m + \eta^T R \eta dt \leq 1 \quad (8)$$

for given symmetric positive-definite matrices  $t \mapsto Q(t)$  and  $t \mapsto R(t)$ ,  $S = Q(0)$ . The MF equations are given by:

$$\begin{aligned} \frac{d\hat{\omega}}{dt} &= A(\hat{\omega})\hat{\omega} + B(t) + PH^T R H (Y - H\hat{\omega}), \hat{\omega}(0) = \omega_0, \\ \frac{dU}{dt} &= -A^T(\hat{\omega})U + H^T R H V, U(0) = I, \\ \frac{dV}{dt} &= Q^{-1}U + A(\hat{\omega})V, V(0) = S^+, P = VU^{-1}. \end{aligned} \quad (9)$$

where  $t \mapsto P(t)$  is the minimax gain and  $S^+$  denotes the pseudoinverse of the matrix  $S$ . Using the implicit midpoint method, the discrete-time form of the last two equations in (9) give the following discrete-time system for obtaining the gain at the  $j + 1$ -th time-level from the gain at the  $j$ -th time-level:

$$\begin{aligned} &\begin{pmatrix} I - \frac{\Delta T}{2} A_j^T & \frac{\Delta T}{2} H^T R H \\ \frac{\Delta T}{2} Q^{-1} & I + \frac{\Delta T}{2} A_j \end{pmatrix} \begin{pmatrix} U_{j+1} \\ V_{j+1} \end{pmatrix} \\ &= \begin{pmatrix} I + \frac{\Delta T}{2} A_j^T & \frac{\Delta T}{2} H^T R H \\ \frac{\Delta T}{2} Q^{-1} & I - \frac{\Delta T}{2} A_j \end{pmatrix} \begin{pmatrix} U_j \\ V_j \end{pmatrix}, \end{aligned} \quad (10)$$

where  $\Delta T$  is the time-step. This time-step must be chosen such that it satisfies a Courant–Friedrichs–Lewy (CFL)-type condition,  $x_i$  and the maximum signal speed,  $\max|f'(\cdot)|$ . The first equation in (9) is also solved using the implicit midpoint method, giving:

$$\begin{aligned} & \left( I + \frac{\Delta T}{2} A_j + \frac{\Delta T}{2} P_{j+1} H^\top R H \right) \hat{\omega}_{j+1} \\ & = \left( I - \frac{\Delta T}{2} B_j - \frac{\Delta T}{2} P_j H^\top R H \right) \hat{\omega}_j + \frac{\Delta T}{2} \frac{P_{j+1} H^\top R Y_{j+1} + P_j H^\top R Y_j}{2}, \end{aligned} \quad (11)$$

which provides the state estimate,  $\hat{\omega}$  at the  $j + 1$ -th time-level using the estimate at  $j$ -th time-level and the gain at both time-levels.

#### D. Qualitative features of MF

Geometrically, the MF approximates the dynamics of the reachability set, which is the set of all states of the model which are compatible with the uncertainty description (8) and observations (7). In other words, the filter describes how the ellipsoid (8) is propagated forward in time by the flow map associated with the model, and the equations (11) describe the evolution of the minimax center of the approximate reachability set of the model.

The convergence of the MF for bilinear systems of the form (6) can be proved for the case of skew-symmetric operator  $A(U)$  which corresponds to the case of the periodic boundary conditions. Specifically, under certain detectability conditions, the equation for the estimation error is asymptotically stable [10]. For non-periodic boundary conditions, the convergence of MF can still be analyzed by the LMI based approach of [10], established for the skew-symmetric operators  $b(\rho) := \rho \rho_x$ : indeed, the non-periodic boundary conditions are treated as sources in the DG approximation of LWR and  $b(\rho)$  is skew-symmetric, provided the test functions vanish at the elemental boundaries.

In the case studied in this article, boundary conditions are not periodic and thanks to the DG formulation, can be treated as source terms. However, the state-transition matrix is not necessarily skew-symmetric. Hence, in section V, we perform an experimental evaluation of the MF by applying its discrete formulation (11) to the real data.

### III. ENSEMBLE KALMAN FILTER FOR LWR MODEL

For comparison purpose, this section describes a TSE approach based on EnKF with the LWR model discretized by the Godunov scheme. It is based on [5] with modifications to the system and observation error matrices, in order to use the highly detailed data for verification. The specification of the model in this method is slightly different—and reported to be better in real-world implementation [5]—than that in the MF. However, by comparing these two filters, practical performance of the MF can be confirmed. In other words, we can compare the two filters at their current best.

#### A. Traffic flow model

The LWR model for velocity (LWR-v) [5] is employed as the system model:

$$\partial_t v(x, t) + \partial_x F(v(x, t)) = 0, \quad (12)$$

where  $v(x, t)$  is traffic speed at time  $t$  and position  $x$ , and  $F$  is a flux function of speed. Note that Eq. (12) and the density-based LWR model (1) describe equivalent traffic if proper flux functions  $F$  and  $f$  were employed; because  $f(\rho(t, x)) = v(t, x)\rho(t, x)$  holds. The following quadratic-linear speed-density function  $V_{\text{QL}}$  is employed:

$$v = V_{\text{QL}}(\rho) = \begin{cases} v_{\text{max QL}} \left( 1 - \frac{\rho}{\rho_{\text{max QL}}} \right), & \text{if } \rho \leq \rho_c, \\ -w \left( 1 - \frac{\rho_{\text{max QL}}}{\rho} \right), & \text{otherwise,} \end{cases} \quad (13)$$

where  $v_{\text{max QL}}$  is a maximum speed,  $\rho_{\text{max QL}}$  is a maximum density,  $v_c$  is a critical speed,  $\rho_c$  is a critical density, and  $w$  is a backward wave speed. This flux function differs slightly from that for the MF (4). Note that the number of the free variables is three, namely,  $v_{\text{max QL}}$ ,  $w$ , and  $\rho_{\text{max QL}}$ ; because  $v_c = v_{\text{max QL}} - w$  and  $\rho_c = \rho_{\text{max QL}} w / v_{\text{max QL}}$  hold to satisfy the continuity of the function.

#### B. Discretized computational scheme for the model

Using the Godunov scheme, Eq. (12) can be discretized as:

$$v_i^{n+1} = V_{\text{QL}} \left( V_{\text{QL}}^{-1}(v_i^n) - \frac{\Delta T}{\Delta X} \left( \tilde{G}(v_i^n, v_{i+1}^n) - \tilde{G}(v_{i-1}^n, v_i^n) \right) \right) \quad (14)$$

with the Godunov flux

$$\tilde{G}(v_1, v_2) = \begin{cases} v_2 \rho_{\text{max QL}} \left( \frac{1}{1+v_2/w} \right), & \text{if } v_c \geq v_2 \geq v_1, \\ v_c \rho_{\text{max QL}} \left( 1 - \frac{v_c}{v_{\text{max QL}}} \right), & \text{if } v_2 \geq v_c \geq v_1, \\ v_1 \rho_{\text{max QL}} \left( 1 - \frac{v_1}{v_{\text{max QL}}} \right), & \text{if } v_2 \geq v_1 \geq v_c, \\ \min \left\{ V_{\text{QL}}^{-1}(v_1) v_1, V_{\text{QL}}^{-1}(v_2) v_2 \right\}, & \text{if } v_1 \geq v_2, \end{cases} \quad (15)$$

where  $\Delta X$  is space discretization width. This is called Cell Transmission Model for velocity (CTM-v) [5]. The CFL condition for CTM-v is  $\max\{v_{\text{max QL}}, w\} \Delta T / \Delta X \leq 1$ .

#### C. Ensemble Kalman Filter

This part briefly summarizes EnKF (adopted from [12]). A state-space model for EnKF can be described as follows

$$\mathbf{z}_n = \mathbf{f}_n(\mathbf{z}_{n-1}, \boldsymbol{\nu}_n), \quad (16)$$

$$\mathbf{y}_n = H_n \mathbf{z}_n + \boldsymbol{\psi}_n, \quad (17)$$

where Eq. (16) is a system equation which is based on the Godunov scheme, Eq. (17) is an observation equation,  $\mathbf{z}_n$  is a state vector,  $\mathbf{f}_n$  is a system model,  $\boldsymbol{\nu}_n$  is a system noise vector,  $\mathbf{y}_n$  is an observation vector,  $H_n$  is an observation matrix, and  $\boldsymbol{\psi}_n$  is an observation noise vector, at time step  $n$  respectively. The observation noise vector  $\boldsymbol{\psi}_n$  follows a normal distribution whose average is 0 and variance-covariance matrix is  $E_n$ , namely,  $\boldsymbol{\psi}_n \sim \mathcal{N}(0, E_n)$ .

The general procedure of EnKF with  $M$  ensemble members can be described as follows:

**Step 1** Generate an ensemble of the initial states  $\{\mathbf{z}_{0|0}^m\}_{m=1}^M$ .  
Let  $n \leftarrow 1$ .

**Step 2** Prediction step:

**Step 2.1** Generate an ensemble of the system noises  $\{\boldsymbol{\nu}_n^m\}_{m=1}^M$ .

**Step 2.2** Calculate  $\mathbf{z}_{n|n-1}^m = \mathbf{f}_n(\mathbf{z}_{n-1|n-1}^m, \boldsymbol{\nu}_n^m)$  for each  $m$ .

**Step 3** Filtering step:

**Step 3.1** Generate an ensemble of the observation noises  $\{\psi_n^m\}_{m=1}^M$ .

**Step 3.2** Obtain the filter ensemble  $\{z_{n|n}^m\}_{m=1}^M$  for each  $m$ , by calculating Eq. (18) based on  $y_n, H_n, E_n, \{z_{n|n-1}^m\}_{m=1}^M, \{\psi_n^m\}_{m=1}^M$ .

**Step 4** Increment the time step,  $n \leftarrow n+1$ . Go back to Step 2 until  $n = n_{\max}$ .

The filter ensemble in Step 3.2 can be derived as follows:

$$z_{n|n}^m = z_{n|n-1}^m + \hat{K}_n \left( y_n + \check{\psi}_n^m - H_n z_{n|n-1}^m \right), \quad (18)$$

where,

$$\hat{K}_n = \hat{V}_{n|n-1} H_n^\top (H_n \hat{V}_{n|n-1} H_n^\top + E_n)^{-1}, \quad (19a)$$

$$\hat{V}_{n|n-1} = \frac{1}{M-1} \sum_{j=1}^M \check{z}_{n|n-1}^j (\check{z}_{n|n-1}^j)^\top, \quad (19b)$$

$$\check{z}_{n|n-1}^m = z_{n|n-1}^m - \frac{1}{M} \sum_{j=1}^M z_{n|n-1}^j, \quad (19c)$$

$$\check{\psi}_n^m = \psi_n^m - \frac{1}{M} \sum_{j=1}^M \psi_n^j. \quad (19d)$$

In this study, the mean of the filter ensemble is taken to be the ‘‘estimation result’’ at time step  $n$ .

The system model,  $f_n$  and  $\nu$ , is based on the CTM-v. In order to integrate the CTM-v into the EnKF framework for TSE, a random noise is introduced to Eq. (14) as follows:

$$v_i^{n+1} = \nu_i^n V_{\text{QL}} \left( V_{\text{QL}}^{-1}(v_i^n) - \frac{\Delta T}{\Delta X} \left( \tilde{G}(v_i^n, v_{i+1}^n) - \tilde{G}(v_{i-1}^n, v_i^n) \right) \right), \quad (20)$$

where  $\nu_i^n$  is a system noise following a uniform distribution between  $1 - \nu$  and  $1 + \nu$ , and is a component of  $\nu^n$ .

The observation model,  $H_n$  and  $\phi_n$ , is constructed as follows. In this study, road-side detectors and GPS-equipped probe vehicles are considered as available sensors, as they are widely used in practical. The detectors are assumed to measure average speed of all the vehicles in each cell in which the sensors are installed with a standard error  $\psi_{\text{detector}}$ . Let  $\delta_i$  be indicator of availability of a detector in cell  $i$ .

The probe vehicles are assumed to measure trajectories of individual vehicles which are randomly sampled with a certain rate. Then the trajectories are converted to average speed  $\hat{v}_i^n$  of probe vehicles in each cell using the generalized definition of traffic state [13]:  $\hat{v}_i^n = \sum_{p \in P_i^n} d_i^n(p) / \sum_{p \in P_i^n} t_i^n(p)$ , where  $P_i^n$  is the set of all probe vehicles,  $d_i^n(p)$  is a distance traveled by probe vehicle  $p$ , and  $t_i^n(p)$  is a time spent by probe vehicle  $p$ , in cell  $i$  at time step  $n$ , respectively. Note that  $\hat{v}_i^n$  may not be identical to  $v_i^n$ , even if the GPS measurement is exact—this is an inevitable measurement error of speed by probe vehicles. This error can be approximated as follows. If  $\Delta X$  is sufficiently smaller than  $\Delta T$ ,  $t_i^n(p) = \Delta T$  holds for most of the vehicles in the cell. This is likely to be satisfied since the cell size must satisfy the CFL condition. Then,

$$\hat{v}_i^n \simeq \sum_{p \in P_i^n} \frac{d_i^n(p)}{t_i^n(p)} = \frac{\sum_{p \in P_i^n} \bar{v}_i^n(p)}{|P_i^n|} \quad (21)$$

holds where  $\bar{v}_i^n(p) = d_i^n(p)/t_i^n(p)$  is the average speed of vehicle  $p$  in cell  $i$  at time step  $n$ . Eq. (21) simply means estimation of the mean of  $\bar{v}_i^n(p)$  for  $p$  for all the vehicles

in the cell based on sampled vehicle set  $P_i^n$ . Therefore, the standard error of  $\hat{v}_i^n$ , namely,  $\psi_{\text{probe}}$ , can be approximated as

$$\psi_{\text{probe}} \simeq \sqrt{\frac{|N_i^n| - |P_i^n|}{|N_i^n|} \frac{\sigma(\bar{v}_i^n(p))}{\sqrt{|P_i^n|}}}, \quad (22)$$

which is a variance estimate from small samples, where  $|N_i^n|$  is a total number of the vehicles in the cell and can be inferred by a density estimate, and  $\sigma(\bar{v}_i^n(p))$  is the standard deviation of  $\bar{v}_i^n(p)$  among the sample set  $P$ .

Since the speed in each cell is both the state and observable variable, a linear observation model with diagonal  $H_n$  can be formulated as follows:

$$h_i^n = \begin{cases} 0, & \text{if } \delta_i = 0 \text{ and } |P_i^n| = 0, \\ 1, & \text{if } \delta_i = 1, \\ 1, & \text{if } \delta_i = 0 \text{ and } |P_i^n| \geq 1, \end{cases} \quad (23)$$

$$\psi_i^n = \begin{cases} 0, & \text{if } \delta_i = 0 \text{ and } |P_i^n| = 0, \\ \psi_{\text{detector}}^2, & \text{if } \delta_i = 1, \\ \psi_{\text{probe}}^2, & \text{if } \delta_i = 0 \text{ and } |P_i^n| \geq 1, \end{cases} \quad (24)$$

where  $h_i^n$  is  $(i, i)$  element of  $H_n$ , and  $\psi_i^n$  is  $(i, i)$  element of  $E_n$ .

## IV. DATA

In this section, specification of the data employed for the empirical verification is summarized.

### A. NGSIM dataset

The NGSIM dataset, publicly provided by [14], is employed for the empirical verification. The specific data in this study contains all of the vehicle trajectories from an actual freeway: a segment of US-101 from 8:09 am to 8:20 am. Total number of observed vehicles was 1938. It contains a on-ramp and an off-ramp. However, the in/out flow from/to the ramps is significantly smaller than the mainline flow; therefore, they are ignored in the estimations. The road segment is 596 m length consists of five lanes except one lane for on/off-ramps. The time resolution of the trajectories is 0.1s. Then Eulerian traffic state with (1s, 16m) time-space resolution (i.e., the time step width and the cell length) is derived from the trajectory data using the generalized definition [13], and is taken as ground truth.

Fig. 2a shows space-mean speed as time–space diagram. According to the figure, the road was partially congested; and clear shockwaves (e.g., backward propagations of jam from the downstream boundary around time 0, 80, and 400 s) can be found. Therefore, the performance of the method in various traffic situations, such as in a free-flow regime, in a congested regime, and with a shockwave can be evaluated.

### B. Sensors

As mentioned, road-side detectors and GPS-equipped probe vehicles are supposed to be available. Their measurements were imitated using the raw dataset. The detectors are assumed to measure flow, density, and speed in each installed cell. The probe vehicles are assumed to measure their trajectory with one second time interval; and then average speed in each cell is inferred by the Edie’s definition.

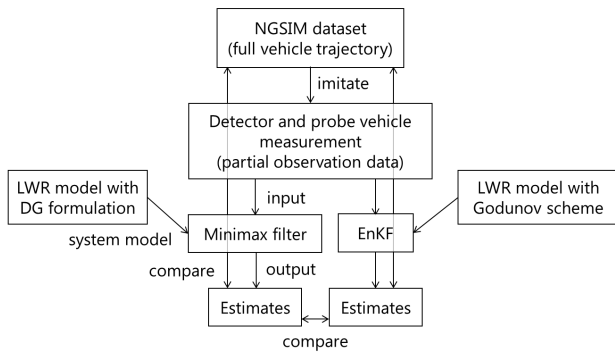


Fig. 1: Comparison scheme of two filters

For the minimax study, the density in a cell with probe vehicles presence is inferred based on the speed-density function and the observed speed:  $\hat{\rho}_i^n = f^{-1}(\hat{v}_i^n)$ .

Following two scenarios on sensors availability are considered:

- 1) Detectors are installed at the upstream and downstream boundaries.
- 2) Probe vehicles are available with 5% penetration rate; and detectors are installed at the upstream and downstream boundaries.

The initial condition (i.e.,  $t = -125$  (s)) was set to be zero because we cannot determine it precisely in practical situations; the area influenced strongly by the initial condition (i.e.,  $t < 0$  (s)) was discarded from the analysis. By comparing the methods using these scenario, the relative accuracy of each method as well as each method's capability of using different measurements can be quantified.

### C. Flux functions calibration

The flux functions are calibrated using data from the same duration and location. This is based on a residual minimization, namely,  $\min_{\theta} \sum_{i \in D} (V(\rho_i; \theta) - \rho_i)^2$ , where  $D$  is a set of cells in each time step whose traffic is near-steady,  $V$  is a flux function,  $\theta$  is a parameters vector to be calibrated, and  $\rho_i$  is density of cell  $i$ . The calibrated parameter values are  $v_{\max} = 20.6$  (m/s) and  $\rho_{\max} = 0.45$  (veh/m) for the minimax and  $v_{\max QL} = 15.2$  (m/s),  $\rho_{\max QL} = 0.70$  (veh/m), and  $w = 4.79$  (m/s) for the EnKF. Note that both flux functions can describe very similar essential features of the traffic. This is because the values of the critical density, which determines whether a traffic is in free-flow or congested regimes, are almost the same for both methods: 0.225 veh/m for the minimax and 0.22 veh/m for the EnKF; in addition, data only contains near-saturated and congested traffic.

## V. VERIFICATION

### A. Specification of filters

Fig. 1 illustrates comparison scheme of the two filters. Both of the filters, namely, MF and EnKF, were applied to the same dataset to estimate the state of the unobserved area.

Technical specification of the filters for the estimation is as follows. First, time and space resolution are  $\Delta T = 1$  (s) and  $\Delta X = 16$  (m). For the MF, we set the number of

elements,  $K = 50$  and use a degree  $N = 2$  basis for DG. Since we do not have any information about errors for this scheme, we set  $Q$ ,  $R$ , and  $S$  each to the identity matrix,  $I$ . In scenario 2, we let the entries of  $R$  vary to reflect the fact that sensors are moving and that some of the locations will become redundant, i.e., if a particular location does not contain a sensor, we set the corresponding entry in  $R$  to reflect the low trust in the measurement in that location. As for the EnKF, the system noise is  $\nu = 0.05$  and the number of the ensembles is 100.

### B. Estimation results

Fig. 2b and c shows the estimation results of scenario 2 using time-space diagrams, where the color maps represent speed, the horizontal axes represent time (the right is the future) the vertical axes represent space (the above is the downstream). According to Fig. 2c, the MF generated several discontinuities which do not exist in the ground truth nor the EnKF results.

Fig. 3 shows snapshots of speed on the road at certain time steps in the scenario 2, where the vertical axes represent space (right is the downstream). Black dots in the figure represent probe vehicle(s) which appear in the cell at the given time step, if their y-coordinates are larger than zero. According to the true state, a backward-moving shockwave, namely, the end of a jam, can be found around  $j = 25$  at  $t = 515$  and  $j = 20$  at  $t = 535$ . At  $t = 535$ , neither filter captured the shockwave as the jam was not well observed. As time progresses, both methods estimate the speed of either side of the shockwave accurately because the number of observations was increased. Oscillations can be found in the estimates by the MF compared to the estimates by the EnKF.

The overall performance of the filters by employing Mean Absolute Percentage Error (MAPE) is as follows: 35.0% for Minimax scenario 1, 36.6% for EnKF scenario 1, 16.7% for Minimax scenario 2, and 12.7% for EnKF scenario 2. According to the result, the MF has slightly better accuracy than the EnKF for the scenario 1. Contrarily, EnKF has better accuracy than the MF for the scenario 2. If we include the area strongly influenced by the zero initial condition for error computation, the MAPEs are 35.3% for Minimax scenario 1, 40.3% for EnKF scenario 1, and 17.5% for Minimax scenario 2, and 13.5% for EnKF scenario 2. This implies that the MF recovers quickly from the wrong initial condition.

### C. Discussion

The minimax state estimator performs well provided the LWR model has been discretized by means of the DG approach, although the physical model error of the LWR model with quadratic flux function is high as evidenced by the scenario 1 (EnKF uses 3 parameters flux function which fit to the data well). The estimation accuracy was significantly improved by additional observation by probe vehicles. Taking the severe model error attributed to the quadratic flux function, the minimax state estimation results for the case of probe vehicles with a moderate number of moving sensors appears to be very promising.

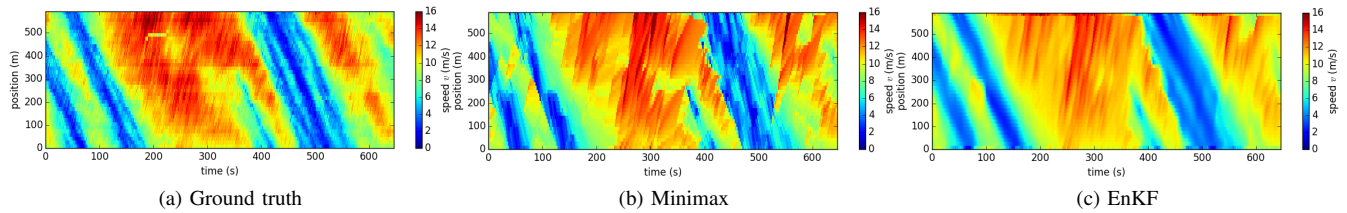


Fig. 2: Speed estimates in scenario 2, visualized as time–space diagrams

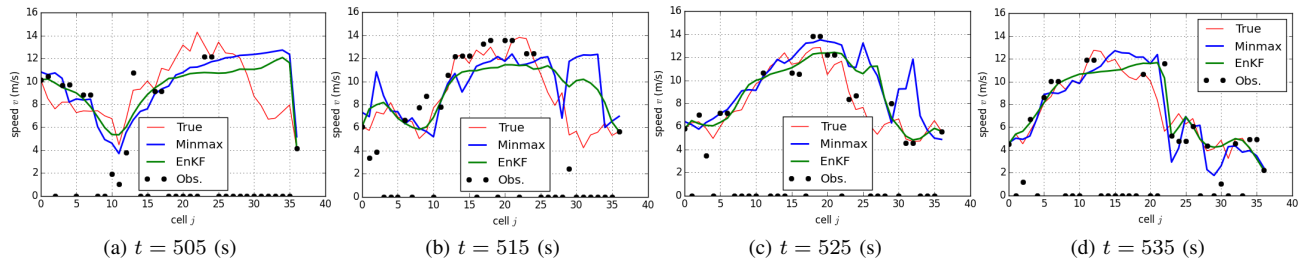


Fig. 3: Speed estimates near a shockwave in scenario 2

The comparison against the EnKF showed that the accuracy of the MF is lower than the EnKF where probe vehicles are present, although it is almost identical to the EnKF where the sensors are limited. One source error in the MF seems to be oscillation and discontinuities in speed estimates. These may be caused by the probe vehicles as the location of discontinuities was close to the trajectories of the probe vehicles. This appears to be due to the rapidly changing error properties and number of available observations. The other reason may be the difference in the flux function. A promising feature of the MF is its quick recovery from the wrong initial condition faster than the EnKF, which is useful in the case when sensors become unavailable for a period of time. In addition, computational cost of the MF is significantly lower than EnKF, which relies on Monte Carlo simulation. This gives MF an advantage over EnKF in the case of highly accurate discretizations (of the LWR model) which are required to deal with complex geometries and quickly varying boundary conditions/sources/observations.

## VI. CONCLUSION

This article represents a first attempt at applying the MF to the LWR model using real traffic data: it has been shown that the MF can be applied to actual traffic with a comparable accuracy to that of EnKF if available sensors are limited. This is a very promising result considering the high model error in the LWR model employed by the MF. By introducing probe vehicles as additional sensors, the accuracy of the MF was improved; however, the improvement was smaller than that of EnKF. This may be due to oscillations of estimates near the probe observations; this issue would be resolved by studying the effect of the time-varying observation matrix. Apart from that, the convergence of the MF for the case of the LWR model with general boundary conditions can be analyzed using the approach of [10] as discussed in section II-D.

## REFERENCES

- [1] Y. Wang and M. Papageorgiou, “Real-time freeway traffic state estimation based on extended Kalman filter: a general approach,” *Transport. Res. B-Meth.*, vol. 39, no. 2, pp. 141–167, 2005.
- [2] M. J. Lighthill and G. B. Whitham, “On kinematic waves. II. a theory of traffic flow on long crowded roads,” *Proceedings of the Royal Society of London. Series A. Mathematical and Physical Sciences*, vol. 229, no. 1178, pp. 317–345, 1955.
- [3] P. I. Richards, “Shock waves on the highway,” *Operations Research*, vol. 4, no. 1, pp. 42–51, 1956.
- [4] C. F. Daganzo, “The cell transmission model: A dynamic representation of highway traffic consistent with the hydrodynamic theory,” *Transport. Res. B-Meth.*, vol. 28, no. 4, pp. 269–287, 1994.
- [5] D. B. Work, S. Blandin, O. P. Tossavainen, B. Piccoli, and A. M. Bayen, “A traffic model for velocity data assimilation,” *Applied Mathematics Research eXpress*, vol. 2010, no. 1, pp. 1–35, 2010.
- [6] G. Evensen, “Sequential data assimilation with a nonlinear quasi-geostrophic model using Monte Carlo methods to forecast error statistics,” *J. Geophys. Res.: Oceans*, vol. 99, no. C5, pp. 10 143–10 162, 1994.
- [7] T. T. Tchrakian and S. Zhuk, “A macroscopic traffic data-assimilation framework based on the Fourier-Galerkin method and minimax estimation,” *Intelligent Transportation Systems, IEEE Transactions on*, vol. 16, no. 1, pp. 452–464, 2015.
- [8] T. T. Tchrakian, S. Zhuk, and A. C. Nogueira, “Robust traffic density estimation using Discontinuous Galerkin formulation of a macroscopic model,” in *IEEE 18th International Conference on Intelligent Transportation Systems*, 2015, pp. 2147–2152.
- [9] S. Zhuk and T. Tchrakian, “Parameter estimation for euler equations with uncertain inputs,” in *Proc. IEEE Conference on Decision and Control*, 2015.
- [10] J. Frank, T. Tchrakian, and S. Zhuk, “Exponentially convergent data assimilation algorithm for Navier-Stokes equations,” ACC2017 (submitted).
- [11] J. Hesthaven and T. Warburton, *Nodal Discontinuous Galerkin Methods: Algorithms, Analysis, and Applications*, ser. Texts in Applied Mathematics. Springer, 2008.
- [12] T. Seo, T. Kusakabe, and Y. Asakura, “Traffic state estimation with the advanced probe vehicles using data assimilation,” in *IEEE 18th International Conference on Intelligent Transportation Systems*, 2015, pp. 824–830.
- [13] L. C. Edie, “Discussion of traffic stream measurements and definitions,” in *Proceedings of the 2nd International Symposium on the Theory of Traffic Flow*, J. Almond, Ed., 1963, pp. 139–154.
- [14] US Department of Transportation, “NGSIM—Next Generation Simulation,” 2006, <http://ops.fhwa.dot.gov/trafficanalysistools/ngsim.htm>, accessed: 2015-02-10.